Report Title:

A Novel Membrane Reactor for Direct Hydrogen Production from Coal

Type of Report: Annual Report

Reporting Period Start Date: 9/9/2003

Reporting Period End Date: 9/30/2004

Principal Authors:
Shain Doong, Estela Ong, Mike Atroshenko, Francis Lau, Mike Roberts

Date Report Issued: October 26, 2004

DOE Award Number: DE-FC26-03NT41851

Submitting Organization:
Gas Technology Institute
1700 South Mount Prospect Road
Des Plaines, IL 60018

DISCLAIMER

ABSTRACT

Gas Technology Institute is developing a novel concept of membrane gasifier for high efficiency, clean and low cost production of hydrogen from coal. The concept incorporates a hydrogen-selective membrane within a gasification reactor for direct extraction of hydrogen from coal-derived synthesis gases. The objective of this project is to determine the technical and economic feasibility of this concept by screening, testing and identifying potential candidate membranes under high temperature, high pressure, and harsh environments of the coal gasification conditions. The best performing membranes will be selected for preliminary reactor design and cost estimates.

To evaluate the performances of the candidate membranes under the gasification conditions, a high temperature/high pressure hydrogen permeation unit has been constructed in this project. The unit is designed to operate at temperatures up to 1100^{o}C and pressures to 60 atm for evaluation of ceramic membranes such as mixed ionic conducting membrane. The unit was fully commissioned and is operational.

Several perovskite membranes based on the formulations of BCN ($BaCe_{0.8}Nd_{0.2}O_{3-x}$) and BCY ($BaCe_{0.8}Y_{0.2}O_{3-x}$) were prepared by GTI and tested in the new permeation unit. These membranes were fabricated by either uniaxial pressing or tape casting technique with thickness ranging from 0.2 mm to 0.7 mm. Hydrogen permeation data for the BCN perovskite membrane have been successfully obtained for temperatures between 800 and 950^{o}C and pressures from 1 to 12 bar. The highest hydrogen flux was measured at 1.6 STPcc/min/cm^{2} at a hydrogen feed pressure of 12 bar and 950^{o}C with a membrane thickness of 0.22 mm.

A membrane gasification reactor model was developed to consider the H_2 permeability of the membrane, the kinetics and the equilibriums of the gas phase reactions in the gasifier, the operating conditions and the configurations of the membrane reactor. The results show that the hydrogen production efficiency using the novel membrane gasification reactor concept can be increased by about 50% versus the conventional gasification process. This confirms the previous evaluation results from the thermodynamic equilibrium calculation.

A rigorous model for hydrogen permeation through mixed proton-electron conducting ceramic membranes was also developed based on non-equilibrium thermodynamics. The hydrogen flux predicted from the modeling results are in line with the data from the experimental measurement. The simulation also shows that the presence of steam in the permeate side or the feed side of the membrane can have a small negative effect on the hydrogen flux, in the order of 10%.

TABLE OF CONTENTS

LIST OF GRAPHICAL MATERIALS

INTRODUCTION

The objective of this project is to develop a novel membrane reactor for high efficiency, clean and low cost production of hydrogen from coal. The concept incorporates a hydrogen-selective membrane within a gasification reactor for direct extraction of hydrogen from coal synthesis gases. This concept has the potential of significantly increasing the thermal efficiency of producing hydrogen, simplifying the processing steps and reducing the cost of hydrogen production from coal. The specific objective of the project is to determine the technical and economic feasibility of using the membrane reactor to produce hydrogen from coal. GTI and our project team (University of Cincinnati, University of Florida and American Electric Power (AEP)) have identified and will evaluate potential membranes (ceramic and metal) suitable for high temperature, high pressure, and harsh coal gas environments. The best performing membranes will be selected for preliminary reactor design and cost estimates. The overall economics of hydrogen production from this new process will be assessed and compared with other hydrogen production technologies from coal.

Our approach to membrane material screening and testing is to first identify the materials that have good thermal stability under the conditions of gasification temperatures. The candidate membranes will be evaluated for their hydrogen flux in a laboratory permeation unit. The acquired data will provide the basis for a preliminary membrane gasifier design, process development and economic analysis. In the next stage of material screening, chemical stability of the membranes with the syngas and its contaminants generated from coal gasification will be evaluated. The trade-off between the hydrogen permeability and chemical stability will be determined.

As coal gasification for hydrogen production occurs at temperatures above 900^{o}C and pressures above 20 atm, it is critically important to evaluate the hydrogen flux of the candidate membrane materials under these operational conditions. To this end, a high pressure/high temperature permeation unit has been constructed. During the first year of the project, the high pressure/high temperature permeation unit has been successfully commissioned. The unit is capable of operating at temperatures and pressures up to 1100^{o}C and 60 atm respectively. The unit will allow screening and testing of the membrane materials at more realistic gasification temperature and pressure conditions. Furthermore, it will be able to demonstrate much higher hydrogen flux from the membranes than what have been reported in the literature.

The mixed proton-electron conducting membrane of the perovskite has been identified as one of the candidate membranes for the membrane gasification reactor applications. The perovskite membrane is 100% selective to hydrogen at high temperatures, >600^{o}C. BCN ($BaCe_{0.8}Nd_{0.2}O_{3-x}$) and BCY ($BaCe_{0.8}Y_{0.2}O_{3-x}$) were first selected for evaluation because they were shown in the literature to have the highest proton conductivity among the perovskite materials. The hydrogen flux obtained in the high-pressure permeation unit will be presented in this report.

To support the conceptual design of the membrane gasification reactor, the required size or dimension of the membrane module for a given operating condition must be determined. A modeling approach is used for this task. Modeling on membrane gasification reactor can also identify key parameters that can affect the performance of the membrane gasification reactor. The findings from the modeling results will be discussed in this report.

To better understand the transport mechanism for the perovskite membrane, a rigorous model based on non-equilibrium thermodynamics and defect chemistry was formulated. This model provides insight on the basic transport mechanism of the proton conducting membranes. The initial results from this modeling effort are summarized in this report.

EXECUTIVE SUMMARY

During the first year of the project, the high pressure/high temperature permeation unit was fully commissioned and is operational. The unit is capable of operating at temperatures up to 1100^{o}C and pressures to 60 atm for evaluation of ceramic membranes such as mixed ionic conducting membranes. The membrane to be tested is in a disk form with a diameter of about 2 cm. A double-seal technique has been developed and tested successfully to achieve leak-tight seal for the tested membranes. Hydrogen permeation data for a commercial Palladium-Gold membrane were obtained at temperatures to 450^{o}C and pressures to 13 bar. The permeation data are consistent with the literature values.

Hydrogen permeation tests for the perovskite membranes have also being performed for both BCN and BCY membranes. These membranes were prepared by GTI using either uniaxial pressing or tape casting technique with thickness ranging from 0.2 mm to 0.7 mm. A total of fifteen samples were tested in the permeation unit. The hydrogen flux for four BCN membranes, one supported with porous layers and three unsupported, were successfully measured. The operating temperatures and pressures are from 800 to 950^{o}C and between 1 and 12 bar respectively. The highest hydrogen flux was measured at 1.6 STPcc/min/cm^{2} at a hydrogen feed pressure of 12 bar and 950^{o}C with a membrane thickness of 0.22 mm.

Both the experimental data and the modeling results show that the hydrogen flux increases with the hydrogen partial pressure in the feed. In addition to the hydrogen partial pressure difference across the membrane, the hydrogen flux also depends on the hydrogen partial pressure in the feed. This may be due to the pressure dependency of proton/electron conductivity of the perovskite materials or more likely the pressure dependency of the proton solubility in the perovskite membranes.

A membrane gasification reactor model was developed to evaluate the H_2 permeability of the membrane, the kinetics and the equilibriums of the gas phase reactions in the gasifier, the operating conditions and the configurations of the membrane reactor. The results show that the hydrogen production efficiency using the novel membrane gasification reactor concept can be increased by about 50% versus the conventional gasification process. This confirms the previous results from the thermodynamic equilibrium calculation.

A rigorous model for hydrogen permeation through the mixed proton-electron conducting ceramic membranes was also developed based on non-equilibrium thermodynamics and defect chemistry. The hydrogen flux predicted from the modeling results are in line with the data from the experimental measurement. The results from the simulation work confirm that the hydrogen flux increases with increasing partial pressure of hydrogen. The presence of steam in the permeate side can have a small negative effect on the hydrogen flux, in the order of 10%. When the steam partial pressure is greater than 1 atm, the hydrogen flux become independent of the steam pressure in the permeate side.

EXPERIMENTAL

High Pressure Permeation Unit

To evaluate the performances of the candidate membranes under the gasification conditions, a high temperature/high pressure hydrogen permeation unit was constructed in this project. The unit was designed to operate at temperatures up to 1100^{o}C and pressures to 60 atm for evaluation of disc membranes with a diameter of about 2 cm. The permeation assembly consists of a tubular permeation cell, a surrounding cylindrical heater, and an enclosing pressure vessel. A simplified schematic illustrating the concept of the permeation cell design is shown in Figure 1. The membrane tested was attached or cemented to a holding tube. A hydrogen feed gas entered through an inner tube in contact with the membrane and exited the system as a non-permeate gas diverted by an outer tube. An inert sweeping gas passing through another inner tube was used to sweep the hydrogen permeate from the membrane. Therefore, the pressure differential across the membrane was insignificant, which would make the membrane sealing less difficult. The two inner tubes and the membrane holding tube are made of Inconel material for its good resistance to heat and easy machining and welding. The ID (inner diameter) of the two inner tubes is 0.62 inch (1.58cm) and the ID of the membrane holding tube is 1.01 inch (2.57 cm). The outer tube is made of Haynes special alloy (HR-160), with an ID of 1.61 inch (4.09 cm). The entire permeation cell assembly was heated by a cylindrical heater, which was enclosed in a pressure vessel purged with an inert gas. The pressure vessel is a flanged 5" Schedule 80 Stainless Steel 316 pipe, with a length of 2 feet.

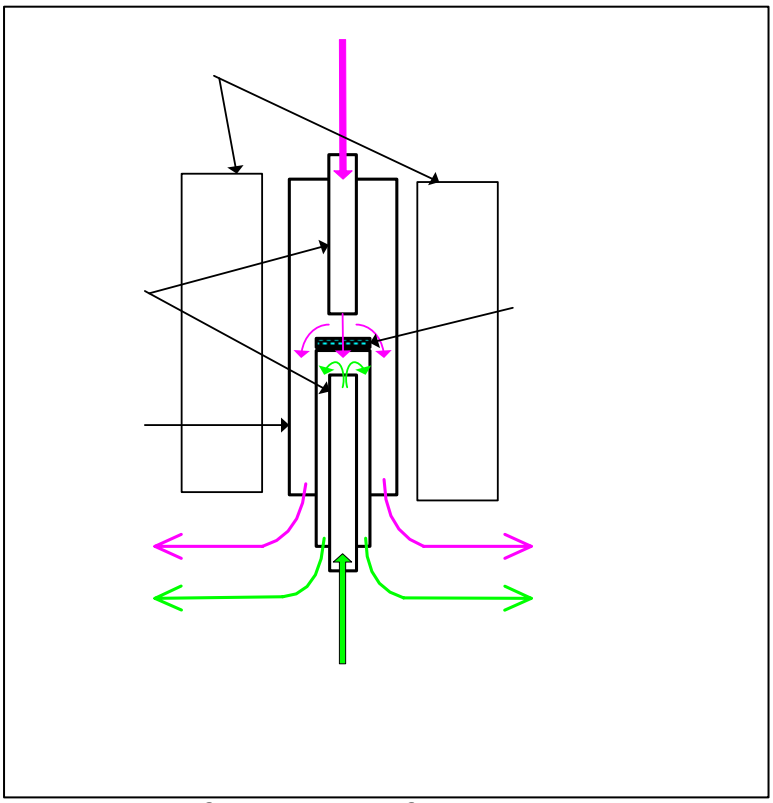

Figure 1. Simplified schematic for the membrane assembly

The entire flow diagram for the high temperature/high pressure permeation unit is shown in Figure 2. All gas flow rates were measured and controlled by the mass flow controllers from Brooks. Although there are three gas inlets into the vessel, feed, purge and sweep gases, all three gas streams eventually vent out of the system through a back pressure regulator, which controls the system pressure and maintains the same pressure for all the three gas streams.

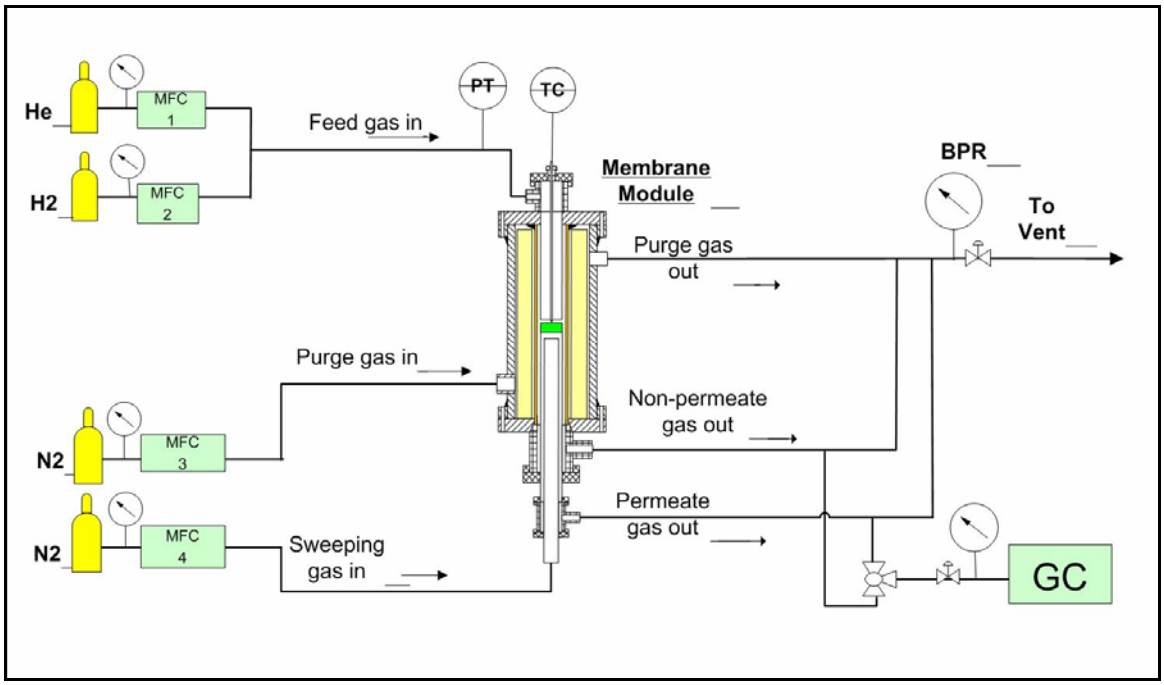

Figure 2. Flow diagram for the high temperature/high pressure permeation unit
MFC: mass flow controller, PT: pressure transducer, TC: thermocouple
BPR: back pressure regulator, GC: gas chromatograph

The hydrogen content of the permeate was analyzed by a Gas Chromatograph (GC) to determine the hydrogen flux through the membrane. Helium and hydrogen were used as the upstream feed gas while nitrogen was used as the down stream sweeping gas. Gas samples were analyzed by a HP 5890 gas chromatograph with a 30-m capillary column packed with molecular sieve 13X. Because it is difficult to separate and detect both hydrogen and helium at the same time by GC, argon was selected as the carrier gas of GC. Nitrogen was also used as the purge gas for the vessel that encloses the heater.

A double-seal technique was developed and tested successfully in the high pressure permeation unit to achieve leak-tight seal for the tested membranes. The membrane to be tested was positioned at the end of a holding tube with a small section of the inner wall cut off to provide additional seal to the membrane, as shown in Figure 3. The membrane was sealed to the tube using two glass tapes in a shape of O-ring, one above and the other below the membrane. The glass sealant material was prepared by mixing glass, perovskite powders, and organic binders. The entire membrane tube assembly was then installed in the permeation unit, first fired to 450^{o}C in air to burn out any organic

compound in the glass tapes, followed by flowing with N_2 to 950°C to melt or soften the sealant. Helium was introduced to the feed side of the membrane while nitrogen was used in the permeate side as a sweeping gas. The absence of helium in the permeate side indicated a good seal and no leakage through the membrane. The tests then proceeded with hydrogen in the feed.

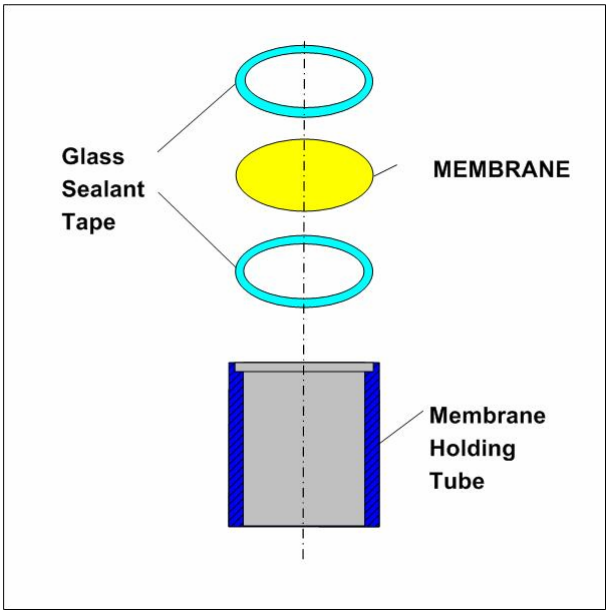

Figure 3. Double-seal design and glass tape provide leak-tight seal for membrane

Membrane fabrication

Cerate-based perovskite membranes of BCN and BCY were the materials selected for evaluation because they were shown in the literature to be one of the highest proton conductive materials among the perovskites. SSC International was contracted to prepare 1 kg each of the powders. The powders possess the required high surface areas (5-10 m^2/g), purity, phase composition and the specified dopant level.

Membrane disks were fabricated by either powder pressing or tape casting technique. Solid BCN and BCY disks with a thickness of 0.045 to 0.07 cm were prepared by pressing powders at 200 atm (3,000 psi) and sintered at 1450 to 1550°C for 2-3 hrs. These unsupported membranes generally are strong and flat. Much thinner (to 0.02 cm) and unsupported membranes were made by using the tape casting technique.

Thin and supported membranes were also made by sandwiching a layer of perovskite powder between two layers of perovskite powders containing about 10 volume percent of a pore former. After pressing and sintering, the middle layer can have a thickness of 0.2 to 0.3 mm. The two outer layers would form the porous supports. Alternatively, the tape casting technique was used to make the supported membranes for the advantages of

flexibility in thickness design, scalability, and cost effectiveness. A thin (0.075 to 0.25 mm) membrane was first made by the tape casting process. Another thick (0.25 to 0.5 mm) membrane tape with 20 volume percent of the pore former was then prepared as a membrane support. The thin membrane was laminated with the thicker porous support to obtain a membrane laminate that is strong enough to handle. Lamination was performed by tape calendaring in which the layers were passed through the rollers. The laminates were then heated to 1450-1550^{o}C range to sinter and densify the membrane layers.

Instead of the organic pore formers used for the porous supports, nickel oxide (NiO) was used as a pore former to create porosity after NiO was reduced to Ni. The reduction process was actually performed in the hydrogen permeation unit by sending hydrogen to both the feed and the permeate sides of the membrane at 950^{o}C for 1.5 hours.

MODELING OF MEMBRANE GASIFICATION REACTOR

To support the conceptual design of the membrane gasification reactor, the required size or dimension of the membrane module for a given operating condition must be determined. A tubular membrane reactor module within a fluidized bed gasifier was used for this modeling study. The free board area or the disengaging zone of a fluidized bed gasifier provides a convenient location for the membrane reactor. Figure 4 is a schematic showing one of the membrane tubes within a fluidized bed gasifier. The coal syngas generated in the gasification zone at the lower section of the fluidized bed enters the membrane reactor module. The membrane tube is assumed to be made of mixed proton/electron conducting perovskite material. Hydrogen will be removed from the tube side of the membrane and the non-permeate will exit the gasifier from the shell side. In this preliminary study, contaminants generated from coal gasification are not considered. In reality, a stable, durable and robust membrane material and the reactor module must be developed.

A mass balance for the feed side of the membrane tube yields

$$\frac{\partial F_i}{\partial x} - R_i + J_i = 0 \qquad (1)$$

where F_i is the molar flow rate of component i, x is the length of the membrane tube, R_i is the reaction rate for forming component i, and J_i is the permeation rate of component i.

To evaluate R_i, chemical kinetics was employed to describe the rates of gas reactions in the feed side of the membrane. This approach was used by Karim and Metwally[1] satisfactorily for modeling of the reforming of natural gas. A reaction scheme comprising 14 chemical species and 32 elemental reaction steps has been employed. The chemical

species considered are six major gas components in the gasifier: CH_4, O_2, CO, H_2, CO_2, and H_2O, and eight radicals: OH, CH_3, H, O, HO_2, H_2O_2, CH_2O, and CHO. Because reforming reactions without catalysts are not expected to occur even at the gasification temperature of 1000°C, catalytic reaction kinetics was used in the model calculations.

In a simplified form, the hydrogen flux can be expressed in the form of the Wagner equation [2,3]:

$$J_{H_2} = -\frac{RT}{4F^2L}\frac{(\sigma_{H^+})(\sigma_{el})}{\sigma_{H^+}+\sigma_{el}}\left(\ln(p_{H_2}^f)-\ln(p_{H_2}^p)\right) \qquad (2)$$

where R is the gas constant, F is the Faraday constant, L is the membrane thickness, σ_{H^+} is the proton conductivity, σ_{el} is the electronic conductivity, $p_{H_2}^f$ is the partial pressure of hydrogen in the feed side of the membrane and $p_{H_2}^p$ is the partial pressure of hydrogen in the permeate side. The values of both proton and electronic conductivity are assumed to be 0.05 S/cm.

Equation (1) can be solved with typical numerical techniques. The required boundary conditions are the flow rates and the compositions of the coal syngas entering the membrane tubes. A GTI gasification model U-GAS is used to estimate the gas flow rates and the compositions from a fluidized bed gasifier, which are listed in Table 1 along with other operating conditions and parameters. The Illinois #6 coal is used for this example.

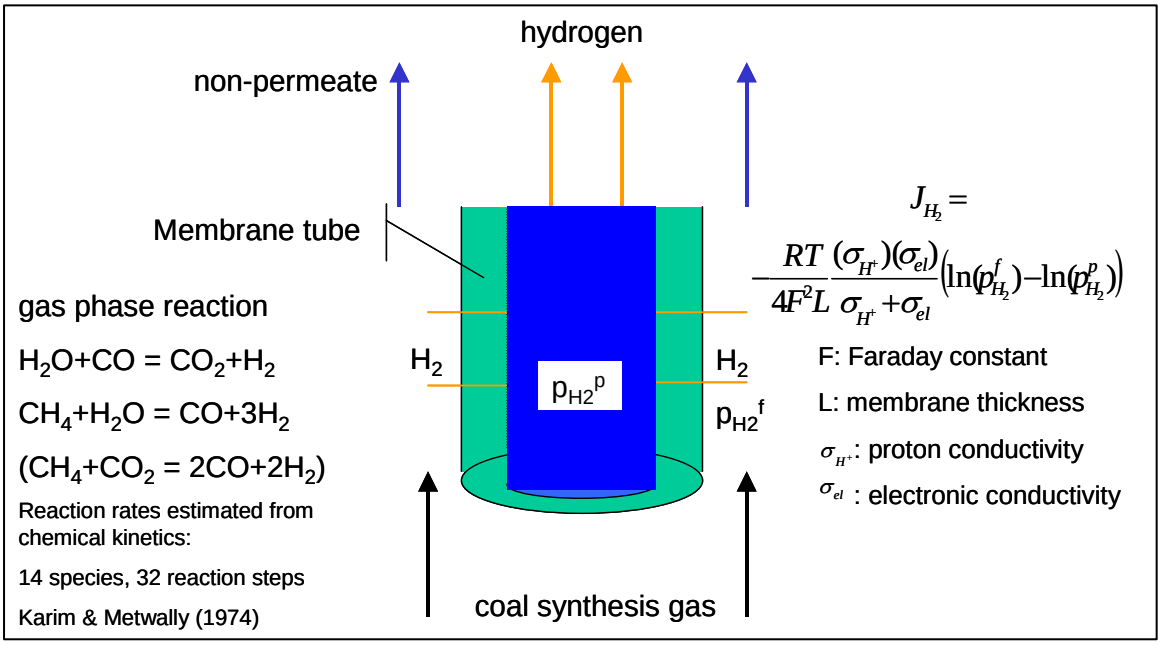

Figure 4. Modeling of a tubular membrane reactor within a gasifier

Table 1. Operating conditions and parameters used in the simulation

coal feed, lb/hr	1000	steam feed to gasifier, lb/hr	595
oxygen feed, lb/hr	534	steam feed to shift reactor,lb/hr	315
temperature, C	1000	coal syngas flow rates, lb/hr	2100
pressure, atm	30	coal syngas composition	
gasifier diameter, cm	50	H_2	0.306
membrane diameter, cm	1.6	CH_4	0.042
membrane thickness, cm	0.002	CO	0.286
membrane length, cm	900	CO_2	0.157
number of membrane tubes	490	H_2O	0.209

MODELING OF MIXED PROTON-ELECTRON CONDUCTING MEMBRANE

A rigorous model for hydrogen permeation through mixed proton-electron conducting ceramic membranes was also developed based on non-equilibrium thermodynamics. The transport of four charged species, proton, oxygen vacancy, electron, and electron hole are described by classical Fick's equation, i.e. flux is proportional to the concentration gradient and the transport coefficient of that species. The concentrations of the species are related to defect chemistry of the perovskite materials and its associated chemical equilibrium. The transport coefficients are determined from the diffusivity, conductivity or mobility measurement. The detailed derivation of the model was given in Appendix. Essentially, a more general form of Wagner equation, Eq. (2), was derived by including contributions from two other defect species, vacancy and electron hole. Furthermore, the conductivities are expressed in terms of species concentrations and diffusivities in the perovskite material, as shown in Eq. (A7).

RESULTS AND DISCUSSION

Hydrogen Permeation Data for Palladium-Alloy Membrane

A commercial Pd-Au membrane with 75 micron in thickness was first tested in the high pressure unit. The membrane was sealed using a high temperature cement, heated to 450^{o}C. Permeation tests were performed at four temperatures, 450, 400, 350, and 300^{o}C at 1 bar. The feed was 50/50 hydrogen/helium with a flow rate of 0.8 SLPM (standard litter per minute). The nitrogen sweeping gas flow was 0.4 SLPM. Operating pressures were also raised from 1 to 13 bar at 300^{o}C. The data are presented in Figure 5. The hydrogen flux in terms of the permeability are in the order of 2~7 x10^{-8} mole/s/m/Pa$^{1/2}$, which are comparable to the typical hydrogen flux of the palladium membranes reported in the literature [4].

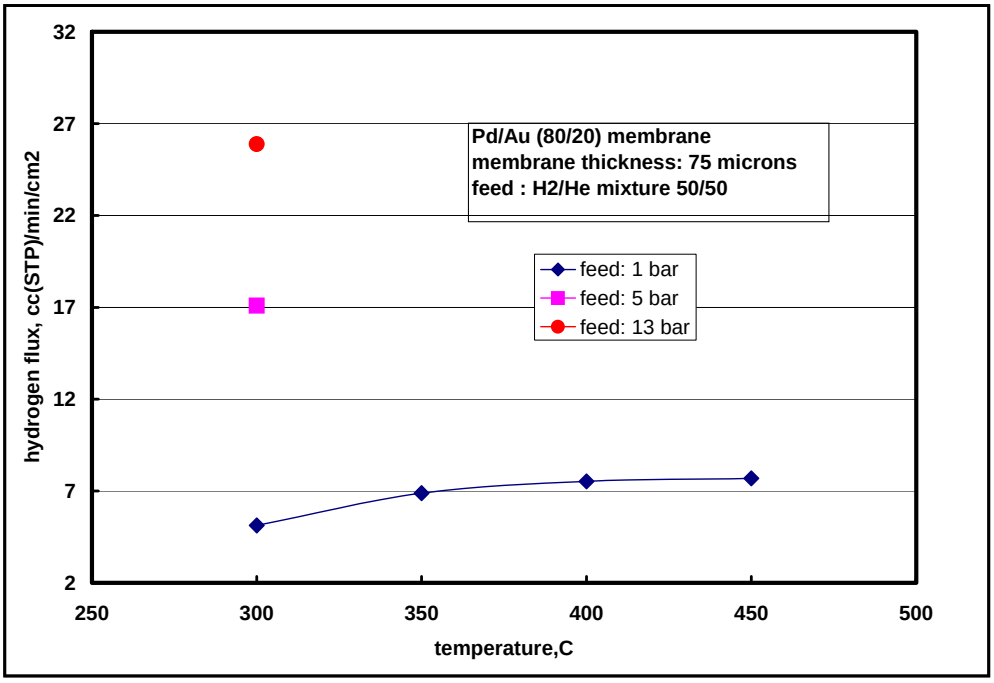

Figure 5. Hydrogen permeation flux for Pd/Au alloy membrane measured from high-pressure permeation unit

Hydrogen Permeation Data for Perovskite Membrane

Fifteen membane samples were tested in the permeation unit. The summary of qualitative testing results are listed in Table 2. The successful tests are considered to have no helium leakage when the feed side was exposed to helium only and to have hydrogen detected in the permeate side when hydrogen was present in the feed side. Three samples showed no hydrogen flux even though they showed no helium leakage. The reasons for those samples to show no measurable hydrogen flux are not clear and still being investigated. The remaining tests, mostly BCY membranes, showed helium leakage. In principle, it is not possible to differentiate whether the leak is from the sealing or the membrane. However, examination of the membrane disks after cool down showed that the membranes had cracks or even broken. Therefore, most of the leakage problems may have come from the membranes instead of the sealing materials.

Table 2. Summary of qualitative testing results from the permeation unit

	Supported membrane	Non-supported membrane
BCN	1 sample: success 1 sample: no H_2 flux	3 samples: success 1 sample: no H_2 flux 1 sample: leak
BCY	4 samples: leak	3 samples: leak 1 sample: no H_2 flux

For the four successful samples, two are unsupported BCN membranes made by uniaxial pressing with thickness of 0.5 and 0.66 mm. The other unsupported membrane, with a thickness of 0.22 mm, was made by tape casting technique. The fourth sample was made by pressing a dense BCN layered between two porous BCN with NiO as a pore former. The dense layer of this supported sample was 0.2 mm.

The hydrogen permeation testing results for the four BCN samples are listed in Table 3. Pure hydrogen was used in the feed for all the tests except one test with 50% of hydrogen in helium. The operating pressures are up to about 12 bar and temperatures to 950C. The feed flow rates were generally in the order of 1000 cc/min. The flow rates of sweeping nitrogen varied from 80 cc/min to about 380 cc/min to generate about 1% hydrogen compositions in the permeate stream. The hydrogen compositions in the permeate side can be changed due to the different sweeping flow rates, which change the term, $\ln(p_{H_2}^f) - \ln(p_{H_2}^p)$, as listed in the last column of Table 3. According to Eq. (2), the hydrogen flux increases with the decreasing hydrogen compositions in the permeate stream because of the increasing driving force of the hydrogen partial pressure between the feed side and the permeate side. However, for the data shown in Table 3, changes of the sweeping flow rates do not significantly affect the hydrogen flux, mainly due to small changes for the value of $\ln(p_{H_2}^f) - \ln(p_{H_2}^p)$.

The hydrogen flux data for the three unsupported BCN membranes are also plotted in Figure 6 against the hydrogen partial pressure in the feed. The hydrogen flux increases with the increasing hydrogen partial pressure in the feed and appears to reach a level-off after about 6 bars. As expected, the hydrogen flux increases with the increasing temperature and the decreasing membrane thickness.

As mentioned, the hydrogen flux is dependent on $\ln(p_{H_2}^f) - \ln(p_{H_2}^p)$ as in Eq. (2). Because of small variations in the values of $\ln(p_{H_2}^f) - \ln(p_{H_2}^p)$ in Table 3, it is difficult to assess this dependency from the available data. Nevertheless, comparing the last two data points from the 0.22 mm unsupported BCN, one with 100% H_2 in the feed at 6 bar and the other with 50/50 H_2/He in the feed at 12 bar, the hydrogen flux is higher for the former case due to a higher value of $\ln(p_{H_2}^f) - \ln(p_{H_2}^p)$.

To eliminate the effect of $\ln(p_{H_2}^f) - \ln(p_{H_2}^p)$ on the hydrogen flux, Figure 7 plots hydrogen flux divided by $\ln(p_{H_2}^f) - \ln(p_{H_2}^p)$ versus hydrogen partial pressure in the feed. According to Eq. (2) or more rigorously Eq. (A17) in the appendix, Figure 7 indicates that the proton and/or electron conductivity depends on the hydrogen partial pressure. The conductivity of the defect species such as proton or electron depends on the concentration and the diffusivity as shown in Eq. (A7). It is not surprising that the concentration of the proton inside the perovskite membrane is dependent on the hydrogen partial pressure. Modeling results, which will be discussed later, also show that the hydrogen flux for the perovskite membrane can not correlate with $\ln(p_{H_2}^f) - \ln(p_{H_2}^p)$ in a linear way. The conductivities of the proton/electron are pressure dependent. Using

Eq.(2) and assuming equal proton and electron conductivity as a first approximation, the proton or electron conductivity is calculated to range from about 0.03 S/cm to about 0.08 S/cm, which are very close to the literature data [9].

Table 3. Hydrogen permeation results for the four BCN samples

	temp, C	pressure, bar	H2 in feed, %	permeate composition H2, %	sweep flow, cc/min	H2 flux, STP cc/min/cm2	Ln(P/feed)-Ln(P/permeate)
unsupported BCN, pressing, 0.5 mm	850	11.5	100	0.999	350	1.31	4.61
	850	6	100	0.925	350	1.21	4.68
	850	1	100	0.854	160	0.51	4.76
	850	1	100	1.487	80	0.45	4.21
	850	1	100	0.418	350	0.54	5.48
unsupported BCN, pressing, 0.66 mm	950	11.9	100	0.384	300	0.65	5.56
	950	8.5	100	0.345	300	0.58	5.67
	950	7.1	100	0.323	300	0.55	5.74
	950	6	100	0.342	300	0.58	5.68
	950	6	100	0.355	300	0.60	5.64
unsupported BCN, tape casting, 0.22 mm	950	12	100	0.917	300	1.61	4.69
	950	6	100	0.892	300	1.57	4.72
	950	4	100	0.784	300	1.38	4.85
	950	1	100	1.203	160	1.13	4.42
	900	1	100	1.090	160	1.03	4.52
	845	1	100	0.858	160	0.80	4.76
	790	1	100	0.733	160	0.69	4.92
	900	12	100	0.695	377	1.53	4.97
	900	12	100	1.070	250	1.57	4.54
	900	6	100	0.626	250	1.38	5.07
	900	12	50	0.774	250	1.13	4.17
supported BCN, pressing, 0.2 mm	900	12.2	100	0.733	295	0.79	4.92
	900	6	100	0.908	250	0.75	4.59
	900	6	100	0.805	200	0.73	4.82
	900	3	100	0.798	200	0.58	4.83
	900	1	100	0.584	160	0.34	6.94
	950	6	100	1.033	250	0.95	4.57
	950	1	100	0.857	160	0.50	6.55

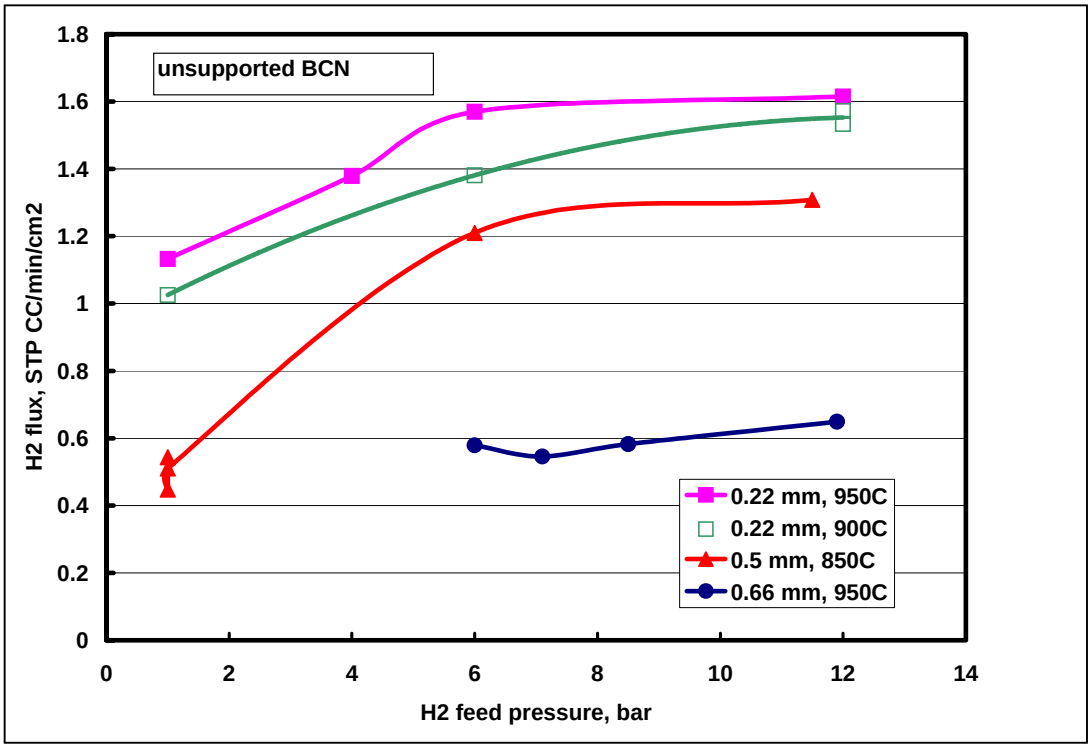

Figure 6. Hydrogen flux versus hydrogen feed pressure for three unsupported BCN membranes

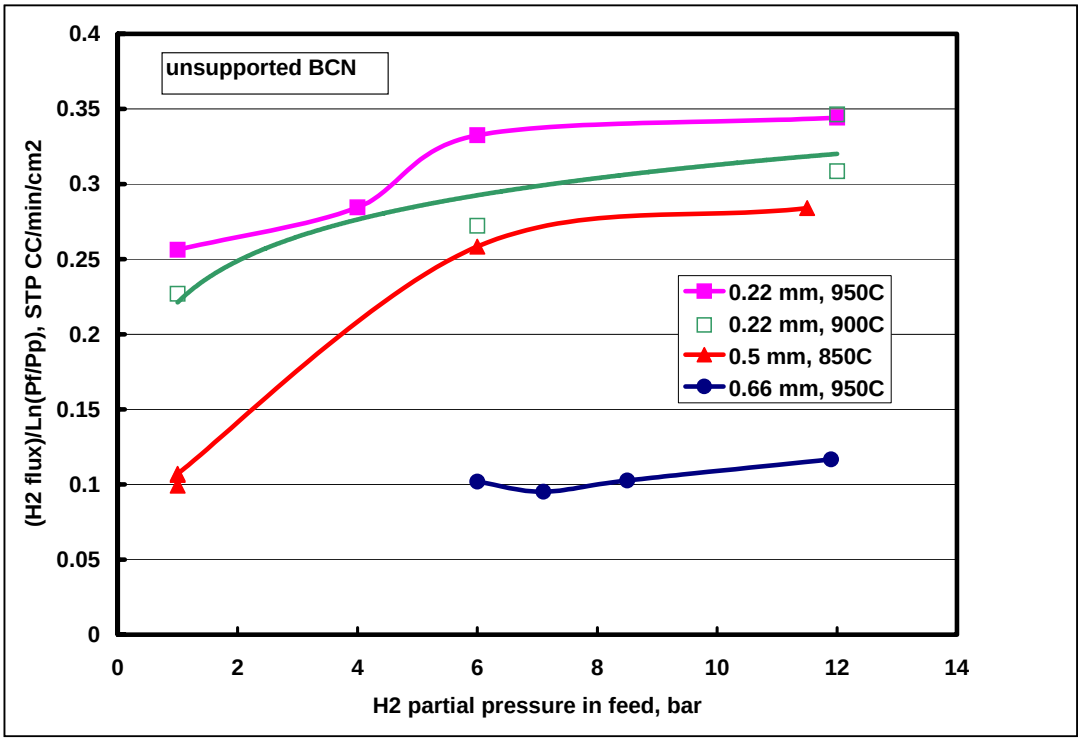

Figure 7. Hydrogen flux divided by Ln(Pf/Pp) versus hydrogen feed pressure for three unsupported BCN membranes

Figure 8 is an Arrhenius plot of the hydrogen flux versus the temperature for the 0.22 mm unsupported BCN membrane at the hydrogen feed pressure of 1 bar. The calculated activation energy is 7.4 Kcal/mole. An activation energy of 12 Kcal/mole for the proton conductivity of BCN material in the presence of steam was reported in the literature [10].

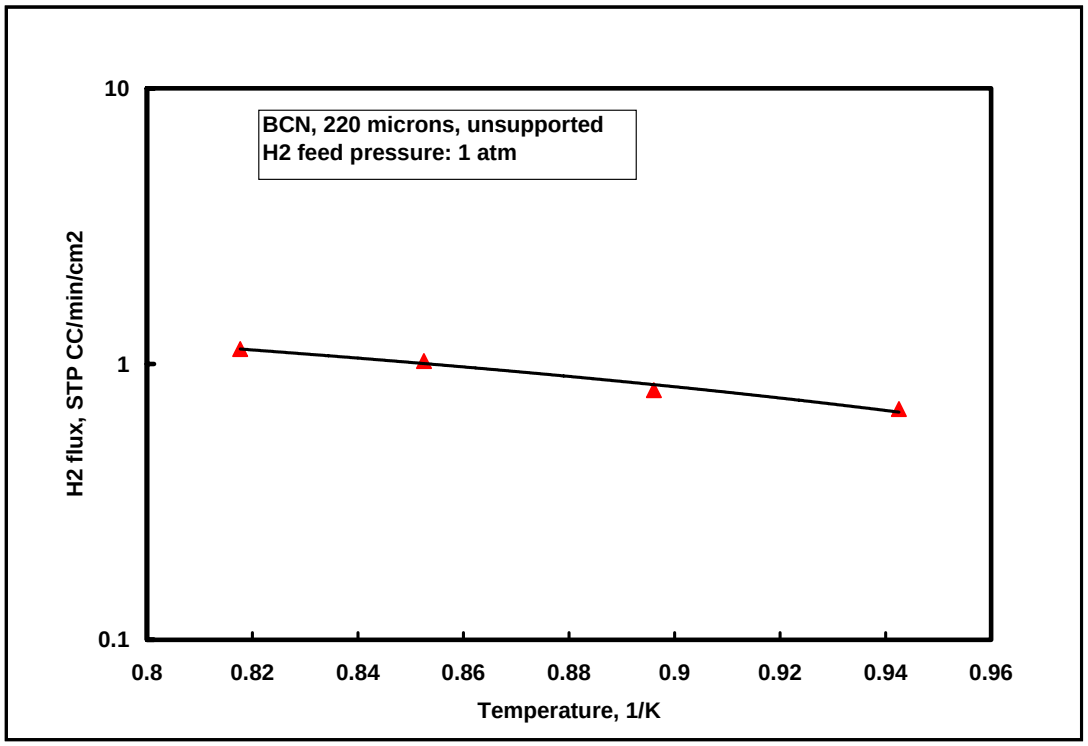

Figure 8. Temperature dependence of hydrogen flux for the BCN membrane

The hydrogen flux for the supported BCN membrane are plotted in Figure 9 for two temperatures at 900°C and 950°C. Compared with the unsupported BCN of 0.22 mm thickness, the supported membrane has lower hydrogen flux. Presumably, the porous support layer could increase the mass transfer resistance and decrease the flux for the supported BCN. As expected, higher temperature increases the hydrogen flux. The curve of the hydrogen flux divided by $\ln(p_{H_2}^f) - \ln(p_{H_2}^p)$ versus hydrogen partial pressure in the feed also shows the same trend as in Figure 7. In addition to $\ln(p_{H_2}^f) - \ln(p_{H_2}^p)$, the hydrogen flux also depends on the hydrogen partial pressure.

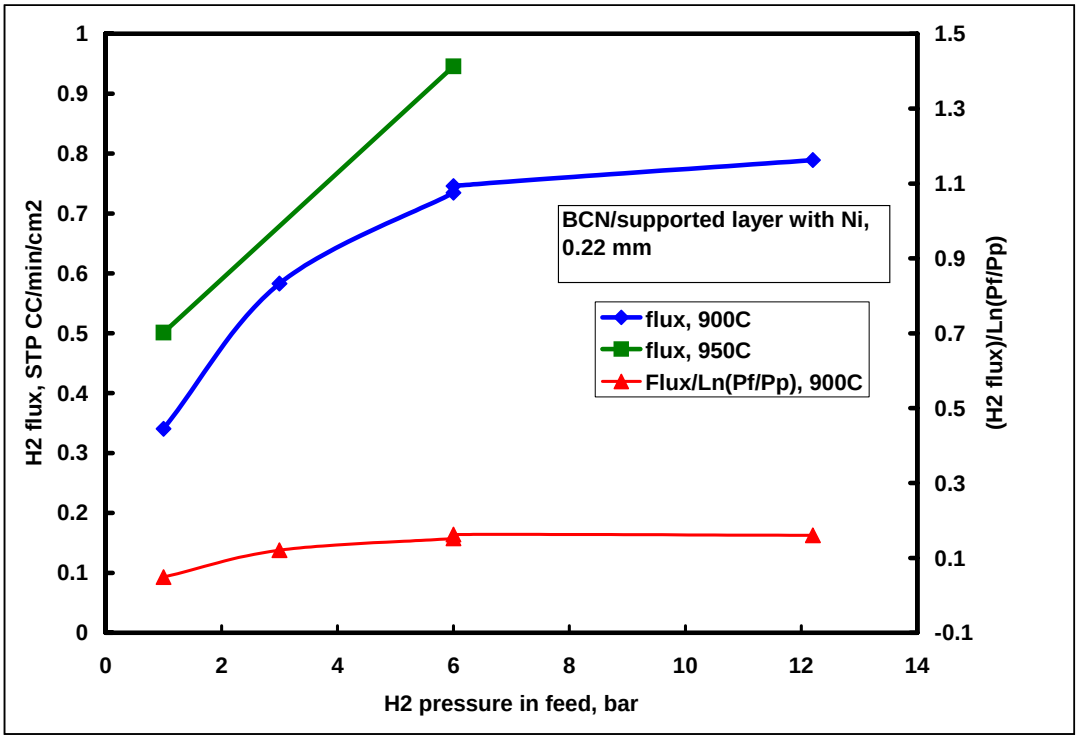

Figure 9. Hydrogen permeation data for the supported BCN membrane

Simulation Results for Membrane Gasification Reactor

Simulation was performed for four different process options for hydrogen from coal gasification, as shown in Figure 10. Process A is the conventional coal to hydrogen process, where a Pressure Swing Adsorption (PSA) is used for hydrogen separation unit. Process B combines the shift reaction and hydrogen separation into a single membrane shift reactor unit. Process C is one of the membrane gasification reactor concept, where hydrogen is directly extracted from the coal gasifier and the non-permeable gas, after clean up, is used for power generation. If the non-permeable gas stream is further processed by a membrane shift reactor to increase the overall hydrogen product, this option of the membrane gasification reactor concept is designated as Process D as shown in Figure 10.

For the conventional coal to hydrogen process, Process A, hydrogen recovery for the PSA unit is assumed to be 80%. The shift reaction is assumed to reach equilibrium at 250^{o}C. If a low temperature membrane shift reactor is used as in Process B and D, the hydrogen is removed to such an extent that the partial pressure of hydrogen in the feed side is reduced to slightly above 1 atm and the shift reaction is at equilibrium. The hydrogen partial pressure in the permeate side is maintained at 1 atm, for both the membrane shift reactor and the membrane gasification reactor.

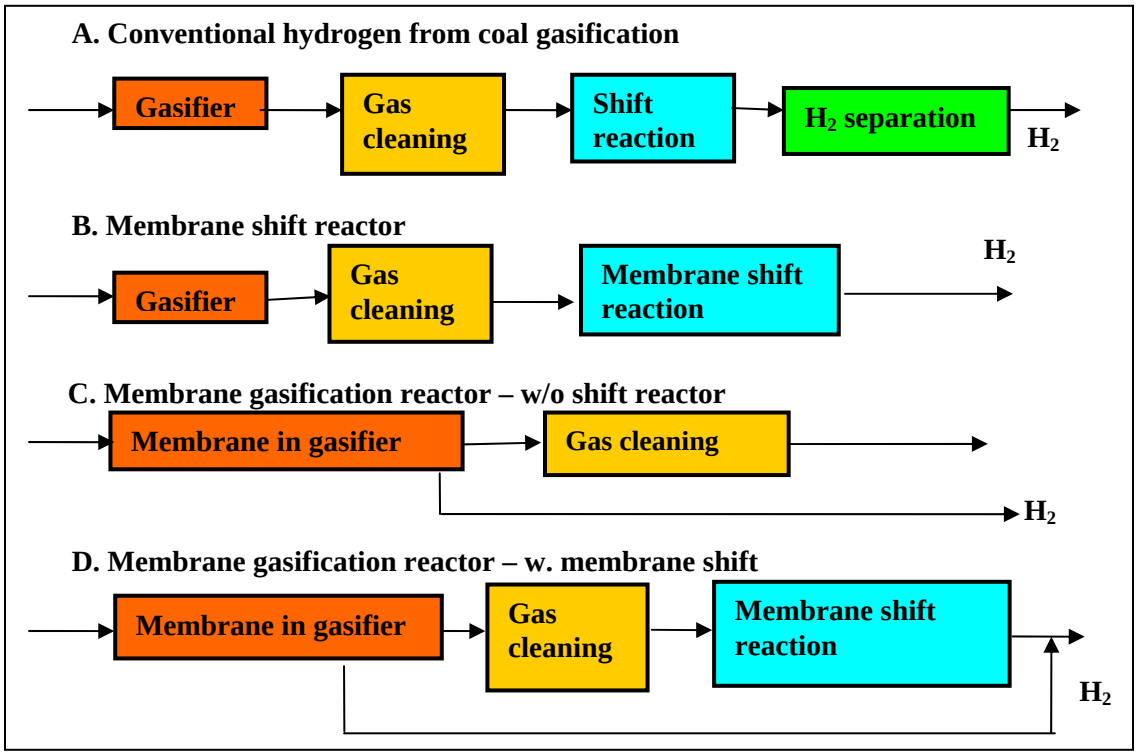

Figure 10. Comparison of Process Options for Hydrogen from Coal Gasification

The results of the simulation are summarized in Table 4 in terms of the number of moles for the hydrogen product and the waste gas or the residual gas. The numbers in Table 4 are all normalized to the hydrogen product for the process A. Process B produces 26% more hydrogen product than Process A because Process B eliminates the hydrogen loss from the PSA tail gas and shifts more CO to H_2 using the membrane shift reactor.

Table 4. Summary of simulation results for the four process options in Figure 10. Catalyzed reactions are assumed for the feed side of the membrane for Process C and D.

Process	A	B	C	D
Hydrogen product, mole	100	126	118	151
Residual gas, mole				
H_2	25	5	6	4
CH_4	9	9	3	3
CO	6	0	33	1
CO_2	92	98	72	103
H_2O	27	21	41	9
to gas clean up	221	221	154	126

As can be seen in Table 4, Process C shows 18% improvement over the conventional process because about two thirds of the methane has been reformed, from 9 to 6. Significant amounts of CO still remain in the non-permeate gas from the membrane gasification reactor because the shift reaction is less favorable at higher temperatures. If the non-permeable stream is sent to a membrane shift reactor at 250^{o}C, as in Process D, all CO can be converted to H_2 and the overall hydrogen product of Process D will be 51% more than Process A. The results confirm the previous evaluation results from the thermodynamic equilibrium calculation.

The gas flows to the gas clean-up section are also listed at the bottom of the Table 4. Process C and Process D significantly reduce the gas amounts sent to the down stream clean-up section. Because Process C does not use low temperature shift reactor, additional steam is added to the gasifier for Process C so that the overall steam fed to the systems are the same for all four processes. Consequently, the amount of gas to the clean-up section for Process C is higher than Process D.

Concentration profiles along the membrane tube for the gas species in the feed side are plotted in Figure 11. As expected, hydrogen and steam mole fractions decrease while CO_2 mole fraction increases. Methane mole fraction also decreases gradually, indicating occurrence of reforming reaction. CO mole fraction increases because the total gas amount decreases due to the permeation of hydrogen through the membrane. The actual component molar flows are plotted in Figure 12, along with the amount of the hydrogen permeating through the membrane. The actual amount of CO in the feed side decreases due to the shift reaction. However, the conversion of CO is very low, at 22%. The high temperature operation, which is unfavorable to the shift reaction, contributes to the low CO conversion. Shift reaction is almost stopped near the end of the membrane reactor, as CO concentration is at its equilibrium value. Moreover, additional CO is also generated by the reforming reactions of methane. The excess amounts of CO can be converted to more hydrogen, if an additional low temperature membrane shift reactor is used, as in Process D.

Both hydrogen mole fraction and hydrogen molar flow rate approach a constant value in Figure 11 and 12 respectively. Because the pressure of the permeate side is kept at 1 atm, the hydrogen mole fraction in the feed side reaches a pinch point and can not be lower than 3.3% for a 30 atm of feed. Even though significant amounts of CO and steam are still present at the membrane reactor outlet, shift reaction has ceased and attained its equilibrium. Consequently, the hydrogen permeation rate is nearly zero toward the end of the membrane outlet. Obviously, reducing the permeate side pressure can increase the hydrogen flux and promote further CO conversion of the shift reaction.

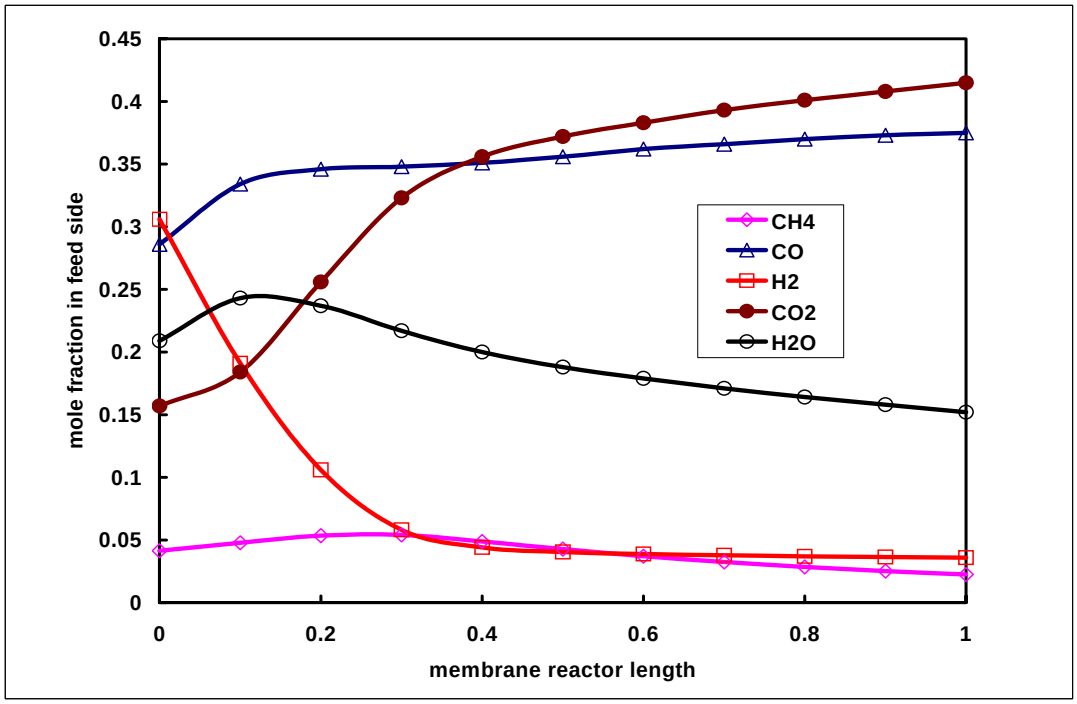

Figure 11. Hydrogen concentration and hydrogen flux at different positions of the membrane as predicted by the model

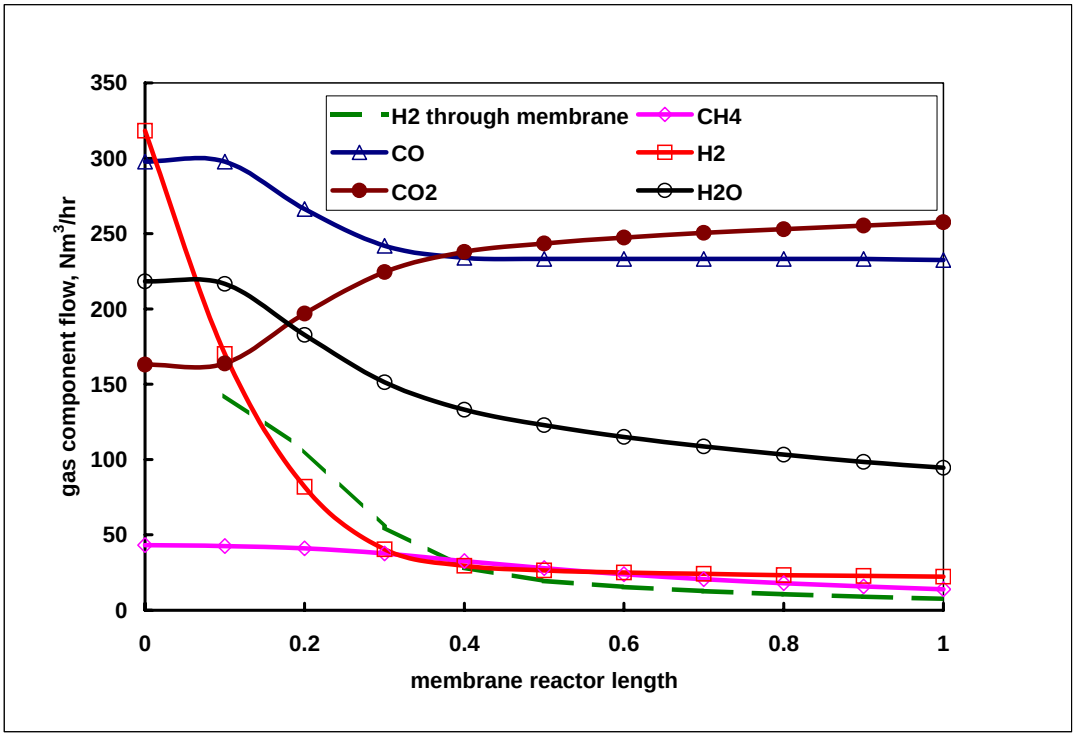

Figure 12. Gas component flow rates in the feed side of the membrane gasification reactor and hydrogen flow through the membrane

Simulation Results for Hydrogen Transport in Mixed Proton-Electron Conducting Membrane

Analysis of hydrogen permeation through a mixed proton-electron conducting membrane was carried out using $SrCe_{0.95}Y_{0.05}O_{3-x}$ (SCY) perovskite membrane. The required physical parameters such as diffusivity and equilibrium constants are taken from the literature [5-8] and are listed in Table 5. Typical concentration profiles for the four major defect species are shown in Figure 13 for a 60/40 hydrogen/steam feed at 20 atm. The permeate side is maintained at 1 atm hydrogen. As seen from Figure 13, both the proton and the electron species dominate in the SCY membrane and the concentrations of the vacancy and the electron hole are very low. The results are reasonable because hydrogen permeation is mainly carried by both the proton and the electron while the vacancy and the electron hole are responsible for the oxygen transport. The proton and the electron concentrations decrease from the feed side to the permeate side as expected. On the other hand, the concentrations of both the vacancy and the electron hole are higher at the permeate side than at the feed side due to less reducing condition of the permeate side.

Table 5 Equilibrium and diffusivity parameters used in the simulation

Equilibrium constant	Value, in mole/cc & atm	diffusivity	Value, cm2/sec
K_1 (Eq. A-9)	$5x10^{-6}$ [8]	proton	$2.19x10^{-3}exp(-5339/T)$ [6]
K_2 (Eq. A-10)	$4.24x10^{-6}exp(14214/T)$ [7]	vacancy	24.24exp(-23467/T) [5]
K_3 (Eq. A-11)	$1.31x10^{-3}exp(29809/T)$ [7]	electron hole	49.38exp(-12589/T) [5]
K_e (Eq. A-15)	$1.x10^{-11}$ [7]	electron	$1x10^{-6}$

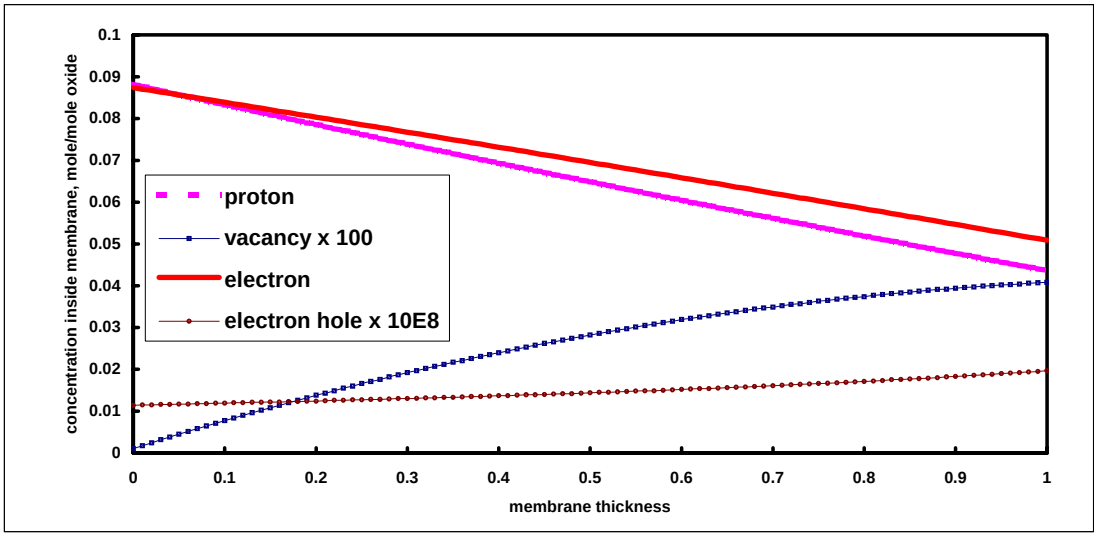

Figure 13. Concentration profiles for the four defect species,, proton, vacancy, electron and electron hole inside a SCY membrane

Simulation was also used to study the effects of the steam partial pressure in the permeate side and the feed side on the hydrogen flux. The presence of steam in the permeate side can reduce the hydrogen flux by about 10% from the very dry conditions. When the steam partial pressure is greater than 1 atm, the hydrogen flux becomes independent of the steam pressure, as shown in Figure 14a. Similarly, the presence of steam in the feed side can reduce the hydrogen flux to a very small effect, as shown in Figure 14b. The presence of steam can generate a small amount of oxygen according to the equilibrium relationship of Eq. (A11). The oxygen molecules can occupy the vacancies of the perovskite structure and increase the oxygen conductivity, which reduces the proton conductivity. In the presence of hydrogen, the effect of steam on the hydrogen flux generally is expected to be small.

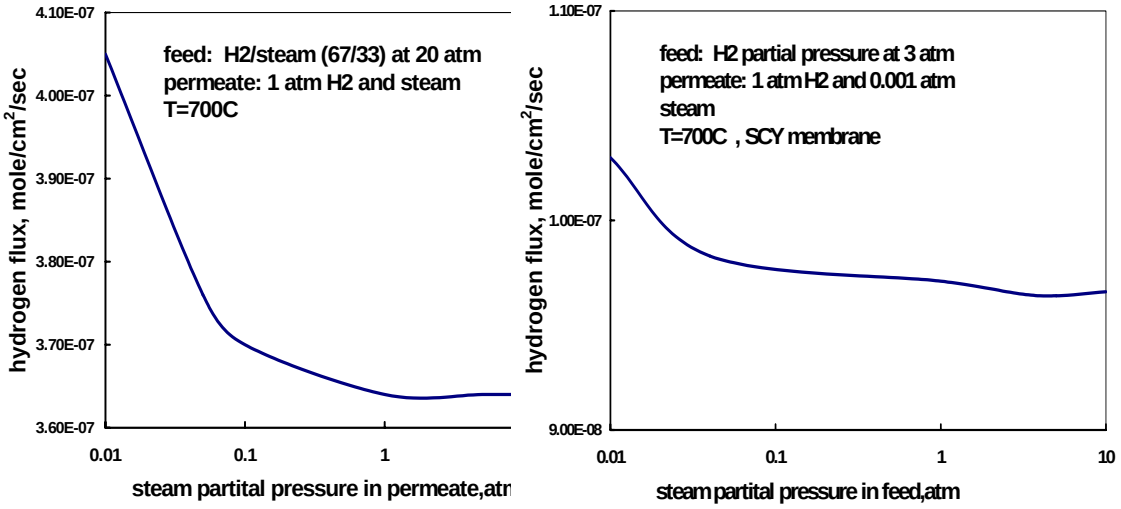

Figure 14. Simulation results show the effects of steam partial pressure a) in the permeate side, b) in the feed side on the hydrogen flux

Simulation was also performed for the experimental conditions used in this work, i.e. pure hydrogen in the feed and about 1% hydrogen in the permeate with the same pressure for both sides of the membrane. The simulation was based on the SCY perovskite membrane and its physical property data as described above. The results are shown in Figure 15 for the hydrogen flux and the hydrogen flux divided by $\ln(p_{H_2}^f) - \ln(p_{H_2}^p)$ versus hydrogen partial pressure in the feed. Compared with Figure 6, the calculated flux are very close to the experimental flux measured in this work, despite different membranes and different operating temperatures used for the experiment and the simulation. Further, the hydrogen flux divided by $\ln(p_{H_2}^f) - \ln(p_{H_2}^p)$ or flux/Ln(Pf/Pp) is not a constant as shown in Figure 15 from the modeling results and in Figure 7 from the experimental data, which indicates that the proton/electron conductivity is dependent on the hydrogen pressure.

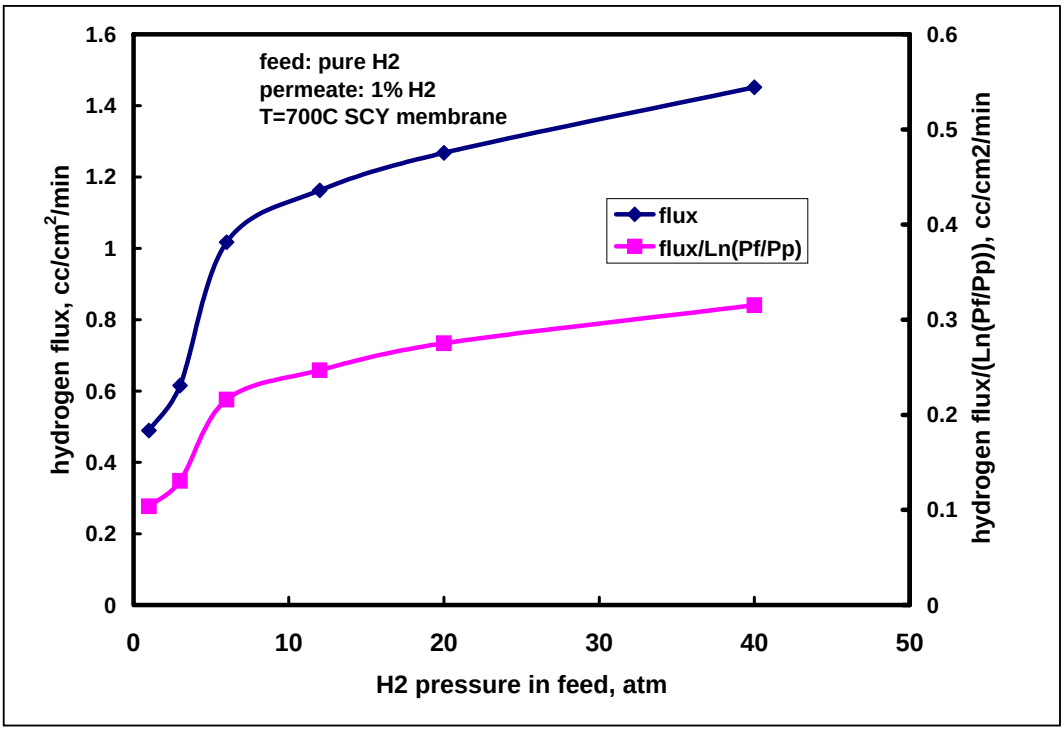

Figure 15. Hydrogen flux as a function of hydrogen pressure in the feed from simulation results

CONCLUSION

The high pressure/high temperature permeation unit is operational and the hydrogen permeation data for the palladium and the perovskite types of membrane have been obtained. Although the flux of the perovskite membrane is almost one order of magnitude lower than the palladium, the perovskite material can operate at higher temperatures suitable for the coal gasification application. The flux can be improved by further reducing the thickness. The highest hydrogen flux was measured at 1.6 STP cc/min/cm^2 at a hydrogen feed pressure of 12 bar and 950^{o}C for a BCN membrane with a thickness of 0.22 mm.

Both the experimental data and the modeling results show that the hydrogen flux increases with the hydrogen partial pressure in the feed. In addition to the hydrogen partial pressure difference across the membrane, the hydrogen flux also depends on the hydrogen pressure in the feed. This may be due to the pressure dependency of the proton/electron conductivity of the perovskite materials or more likely the pressure dependency of the proton solubility in the perovskite membranes.

The modeling results show that the hydrogen production efficiency using the novel membrane gasification reactor concept can be increased by about 50% versus the

conventional gasification process. A rigorous model for hydrogen permeation through mixed proton-electron conducting ceramic membranes was also developed. The hydrogen flux predicted from the modeling results are in line with the data from the experimental measurement.

PLAN FOR NEXT YEAR

Hydrogen permeation testing for the perovskite membranes will be continued on the permeation unit under typical gasification temperature and pressure conditions. Current plan will test the following cerate-based perovskite membranes:

- Supported ultra-thin membranes prepared by either tape casting or uniaxially pressing.
- Membranes prepared from University of Cincinnati
- Membranes based on perovskite powders supplied from University of Florida
- Dual phase cermet materials incorporating Pd, or Ni in the perovskite structure

Having established the baseline performance for the perovskite membranes, the next stage of the membrane development effort will focus on the chemical stability issues of the perovskite membrane.

Based on the hydrogen permeation data and modeling approach, a conceptual design of membrane gasifier configuration for a plant of 1000 TPD coal will be conducted (Task 2). The objective is to determine if the perovskite membranes have sufficient flux to be used for the membrane gasification reactor design.

Flowsheet simulation for hydrogen production from coal based on the membrane gasifier processes will be performed (Task 3). At the end of the project, we will complete technical and economical assessment of the proposed membrane gasifier technology (Task 4).

REFERENCES

1. G.A. Karim and M.M. Metwally "A Kinetic Investigation of the Reforming of Natural Gas for the Production of Hydrogen", Int. J. Hydrogen Energy, Vol. 5, pp 293, 1979
2. H.J.M. Bouwmeester and A.J. Burggraaf "Dense ceramic membranes for oxygen separation", in Fundamentals of Inorganic Membrane Science and Technology, Ed. By A.J. Burggraff and L. Cot, pp 435-528, 1996, Elsevier Science B.V.
3. T. Norby and Y. Larring "Mixed hydrogen ion-electronic conductors for hydrogen permeable membranes", Solid State Ionics, 136-137, pp139-148, 2000
4. B.D. Morreale,M.V. Ciocco, R.M. Enick, B.I. Morsi, B.H. Howard, A.C. Cugini, K.S. Rothenberger "The permeability of hydrogen in bulk palladium at elevated temperatures and pressures", J. of Membrane Science, 212, pp87-97, 2003
5. X. Tan, S. Liu, K. Li and R. Hughs "Theoretical analysis of ion permeation through mixed conducting membranes and its application on dehydrogenation reactions", Solid State Ionics, 138, pp149-159, 2000
6. T. Schober, J. Friedrich, and J.B. Condon, "Effective hydrogen diffusivity in $SrCe_{0.95}Yb_{0.05}O_{3-a}$ and $SrZr_{0.95}Yb_{0.05Y}b0.05O_{3-a}$, Solid State Ionics, 77 pp175-179, 1995
7. T. Schober, W. Schilling and H. Wenzl "Defect model of proton insertion into oxides", Solid State Ionics, 86-88, pp653-658, 1996
8. S-J Song, E.D. Wachsman, J. Rhodes, S.E. Dorris, U. Balachandran "Numerical modeling of hydrogen permeation in chemical potential gradients", Solid State Ionics, 164, pp107-116, 2003
9. H. Iwahara, H. Uchida, K. Ono and K. Ogaki "Proton Conduction in Sintered Oxides Based on $BaCeO_3$", J. Electrochem. Soc.: Solid-State Science and Technology, V135, No 2, pp529, 1988
10. J.F. Liu and A.S. Nowick, "The incorporation and migration of protons in Nd-doped $BaCeO_3$", Solid State Ionics, 50, pp131, 1992
11. L. Li and E. Iglesia "Modeling and analysis of hydrogen permeation in mixed proton-electronic conductors", Chem Engr Sci, 58, pp1977-1988, 2003

APPENDIX

In a MIEC membrane, the driving forces for the transport of charged species come from both chemical and electrical potential gradients. The flux of each species k, J_k can be described by a combination of Fick's law and the equation for ion migration:

$$J_k = -\frac{\sigma_k}{z_k^2 F^2}\left(\frac{\partial \mu_k}{\partial x} + z_k F \frac{\partial \phi}{\partial x}\right) \quad \text{(A1)}$$

where μ is the chemical potential, ϕ is the electrical potential, σ is the conductivity, z is the charge number and F is the Faraday constant.

When no external current is imposed on the membrane, the net flux from all the charged species is zero, i.e.

$$I = \sum_{k=1}^{n} I_k = \sum_{k=1}^{n} z_k F J_k = 0 \quad \text{(A2)}$$

Combining Eqs.(A1) and (A2), a relationship between the electrical potential and the chemical potential can be obtained:

$$\frac{\partial \phi}{\partial x} = -\sum_{k=1}^{n} \frac{t_k}{z_k F} \frac{\partial \mu_k}{\partial x} \quad \text{(A3)}$$

where t_k is the transport number of species k, which is a relative measure of conductivity of species k to the total conductivity.

$$t_k = \frac{\sigma_k}{\sum_{i=1}^{n} \sigma_i} \quad \text{(A4)}$$

The flux equation, Eq. (A1) now becomes

$$J_k = -\frac{\sigma_k}{z_k^2 F^2}\left(\frac{\partial \mu_k}{\partial x} - z_k \sum_{i=1}^{n} \frac{t_i}{z_i} \frac{\partial \mu_i}{\partial x}\right) \quad \text{(A5)}$$

Chemical potential μ is related to chemical activity a_i by

$$\frac{\partial \mu_k}{\partial x} = RT \frac{\partial \ln a_k}{\partial x} \tag{A6}$$

Under ideal conditions, the activity a can be substituted with the concentration C. Further, the conductivity of the defect species can be correlated with its concentration and diffusivity by the Nernst-Einstein equation:

$$\sigma_k = \frac{z_k^2 F^2}{RT} C_k D_k \tag{A7}$$

Substituting Eq.(A6) and (A7) into Eq.(A5), the following equation can be obtained:

$$J_k = -C_k D_k \left[\frac{(1-t_k)}{C_k} \frac{\partial C_k}{\partial x} - \sum_{\substack{i=1 \\ i \neq k}}^{n} \frac{z_k t_i}{z_i C_i} \frac{\partial C_i}{\partial x} \right] \tag{A8}$$

Eq. (A8) relates the flux of each species to the concentrations and the diffusivities of all the species inside the MIEC membrane.

In proton-electron conductors, charged carriers are protons ($OH^{\bullet}$), vacancies ($V_{\ddot{O}}$), electrons (e^{-}), and electron holes ($h^{\bullet}$). The concentrations of the defect species in a typical proton conductor can be described by the following stoichiometric equations [11]:

$$1/2 O_2 + V_{\ddot{O}} = O_O^x + 2h^{\bullet} \qquad K_1 = C_h^2 \Big/ \left(C_V \, p_{O_2}^{1/2} \right) \tag{A9}$$

$$H_2 + 2O_O^x = 2OH^{\bullet} + 2e^{-} \qquad K_2 = \left(C_{OH}^2 C_e^2 \right) \Big/ p_{H_2} \tag{A10}$$

$$H_2 + 1/2 O_2 = H_2O \qquad K_3 = p_w \Big/ \left(p_{H_2} \, p_{O_2}^{1/2} \right) \tag{A11}$$

where O_O^x denotes the lattice oxygen. Eqs.(A9) to (A11) establish the relationships between the concentrations of charged species inside the membrane to the gas partial pressures outside the membrane. The chemical potentials of each charged species can also be related to the chemical potentials of gases through the following equations corresponding to Eqs.(A9) to (A11):

$$1/2 \mu_{O_2} + \mu_V = 2\mu_h \tag{A12}$$

$$\mu_{H_2} = 2\mu_{OH} + 2\mu_e \tag{A13}$$

$$\mu_{H_2} + 1/2\mu_{O_2} = \mu_w \tag{A14}$$

Also the electronic equilibrium requires

$$e^- + h^\bullet = nil \qquad K_e = C_e C_h \tag{A15}$$

$$\mu_e + \mu_h = 0 \tag{A16}$$

Therefore, Eq.(A8) for proton $OH^\bullet$ and vacancy $V_{\ddot{O}}$, will become

$$J_{OH} = -\frac{t_{OH}\sigma RT}{2F^2}\left[\left(t_h + t_e\right)\frac{\partial \ln p_{H_2}}{\partial x} + 4t_V\sigma\frac{\partial \ln p_w}{\partial x}\right] \tag{A17}$$

$$J_V = -t_V\sigma\frac{RT}{F^2}\left[\left(t_h + t_e\right)\frac{\partial \ln p_{H_2}}{\partial \ln x} - \left(t_h + t_e + t_{OH}\right)\frac{\partial \ln p_w}{\partial x}\right] \tag{A18}$$

Eqs.(A17) and (A18) can not be integrated directly because the transport numbers, t_i and the total conductivity σ are functions of the membrane position x. However, at steady state, J_{OH} and J_V are constant and independent of the membrane positions. The above equations can be rearranged to give

$$\frac{RT}{F^2}\frac{\partial \ln p_{H_2}}{\partial x} = -\frac{4J_V}{\sigma\left(t_h + t_e\right)} - \frac{2J_{OH}\left(t_h + t_e + t_{OH}\right)}{\sigma t_{OH}\left(t_h + t_e\right)} \tag{A19}$$

$$\frac{RT}{F^2}\frac{\partial \ln p_w}{\partial x} = \frac{J_V}{\sigma t_V} - \frac{2J_{OH}}{\sigma t_{OH}} \tag{A20}$$

Given the boundary conditions at both the feed side and the permeate side of the membrane, Eqs.(A19) and (A20) can be integrated with respect to x to obtain the profiles of hydrogen and water partial pressures across the membrane. The concentration profiles of the four defect species, proton $\left(C_{OH}\right)$, vacancy $\left(C_V\right)$, electron $\left(C_e\right)$, and electron hole $\left(C_h\right)$ are related to the gas partial pressure through Eqs.(A9) to (A11). The required parameters for the membrane material are equilibrium constants, $K_1, K_2, K_3,$ and K_e as well as the diffusivity data for the four defect species.